12.2

DEVELOPMENT OF SATELLITE-BASED CLOUD TOP HEIGHT AND CONVECTION NOWCASTING PRODUCTS IN SUPPORT OF SIGMET COORDINATION IN APAC REGION

Christy Y. Y. Leung*, H.C. Tam, W.S. Chan, and H.K. Fok

Hong Kong Observatory, Hong Kong, China

1. INTRODUCTION

The International Civil Aviation Organization (ICAO) has been promoting regional coordination in the provision of Significant Meteorological Information (SIGMET) in the Asia Pacific (APAC) region. Following the Conclusion APANPIRG/28/30 on encouraging States to participate in cross Flight Information Region (FIR) boundary SIGMET coordination, a few SIGMET coordination projects were set up aiming to providing harmonized hazardous weather information for the benefits of aviation users.

The Hong Kong Observatory (HKO) has developed a web platform for Meteorological Watch Offices (MWOs) in the APAC region to support their operations in preparing harmonized SIGMET across neighboring FIRs since 2016 The platform provides a suite of weather information, including satellite, radar, lightning, wind field, latest SIGMET, etc. graphical information, to provide common-situational-awareness to the platform users. Noticing that a few essential parameters, namely cloud top height, convection intensity and the respective nowcast of the deep convection are essential piece of information for forecasters in the preparation of SIGMET, HKO conducted several researches and made a few enhancements on the HKO SIGMET coordination web platform to support the forecasters' daily operations in terms of WS SIGMET (Thunderstorm SIGMET) issuance.

This paper discusses the algorithms developed for improving cloud top height estimation and the satellite derived radar reflectivity used for intensity estimation of significant convection. Comparison of the performance of different algorithms are also discussed.

2. CLOUD TOP HEIGHT ALGORITHM

2.1 Methodology

Cloud top height (CTH) represents the vertical extent of a deep convection cloud which is useful for flight tactical and strategic planning. CTH is one of the essential parameters in a WS SIGMET message. CTH can be estimated by plugging the brightness temperature from a satellite via Eq (1),

$$P = P_o \left(\frac{T}{T_o}\right)^{\frac{g}{LR}} \quad (1)$$

where g is the gravitational acceleration, R the ideal gas constant, L atmospheric lapse rate, T_o surface temperature and P_o pressure. The corresponding flight level (FL) is converted from P to FL according to the Manual of ICAO Standard Atmosphere [1].

(a) Climatological algorithm

Noting that L in Eq. (1) varies with place, height and season while T_o may not be available over many areas under the satellite image area, a simple climatological approach was examined by collecting upper air soundings of coastal and low elevated stations in the region in 2016. From the profiles, the lapse rate L were plotted as functions of latitude, altitude and month. A total number of 60 charts spanning from January to December, for the region between 40°N to 20°S, in 5 layers were compiled (samples in Figure 1). Similarly, temperature *To* was also plotted as functions of latitude and month. It is found that both L and *To* behave as quadratic functions w.r.t. latitude and/or height. In Eq (1), P_o was chosen to be 500hPa to minimize localized topographic effects of temperature near the surface.

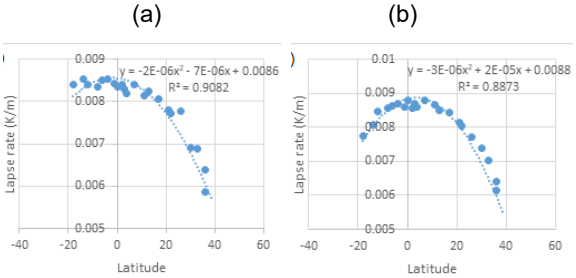

Figure 1: Samples of Lapse rate (L) between 250hPa and 200hPa against latitude in (a) April and (b) October. The fitting equation and R^2 value are also shown.

By using the above climatological lapse rate L and reference temperature *To* charts, cloud top pressure was estimated by Eq. (1) with the CTH derived using ICAO standard atmosphere. The utilization of the climatological approach on satellites can cater for areas where there are sparse sounding observations.

Although the above climatological approach could improve the latitudinal and seasonal variation effects, several limitations remain. For example, as this approach only takes soundings over land stations in tropics and subtropics (within 40°N and 20°S) into account, its validity beyond this domain and over sea areas are questionable. Meanwhile, as only one morning and one evening sounding were available,

* *Corresponding address:* Christy Y.Y. Leung, Hong Kong Observatory, 134A Nathan Road, Tsim Sha Tsui, Hong Kong, China; email: yyleung@hko.gov.hk

how far this method could be used for a storm developing in between is also doubtful.

(b) ECMWF model-based algorithm

Another approach to determine CTH from satellite is to utilize numerical weather prediction (NWP) models' outputs, e.g. [2]. Temperature and dew point profiles extracted from ECMWF with data resolution of 0.125° were used in our development. The temporal resolution of the model output used in the study was hourly. A cloud top height could then be estimated from the cloud top temperature obtained from the satellite brightness temperature of the infrared channel in comparison with that from the model. As the temperature measured by the satellite could lie between model levels, the corresponding pressure level *P* was obtained through linearly interpolating from the model logP-T diagram (Figure 2). Assuming that the cloud top height would not exceed the tropopause, the highest level on the diagram that corresponds to the brightness temperature was chosen. The cloud top height in terms of *FL* can then be estimated following para. 2.1. Note that the cloud top temperature can be measured by the two brightness temperature at Band 13 (10.4μm) or 14 (11.2 μm) [3]. We included the CTH retrieved by both Bands in the comparison to assess which one is more reliable.

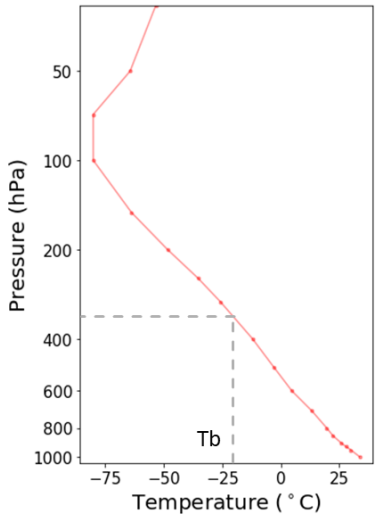

Figure 2: Schematic diagram of how to obtain *P* pressure using Tb satellite brightness temperature from ECMWF vertical profile.

(c) EUMETSAT/NWC SAF

A further algorithm that we have studied is the satellite application facilities (SAFs) of the EUMETSAT [4]. The CTH algorithm in SAF uses the RTTOV radiative transfer model [5] applied on NWP vertical profile to simulate the satellite radiances and brightness temperatures. Then, various retrieval methods of CTH (e.g. radiance ratioing technique) for various cloud types were applied. Through collaborative work with the SAF/NWC team, HKO has adapted the SAF cloud algorithms for Himawari-8 satellite via tuning of the look up tables in clear skies utilizing the RTTOV and ECMWF NWP model. Routine production of the SAF cloud products based on Himawari-8 has been implemented in the Observatory since 2017.

2.2 Verification

(a) Objective performance comparison

The performance of the above algorithms was objectively evaluated against the data obtained from the Cloud-Aerosol Lidar and Infrared Pathfinder Satellite Observation (CALIPSO). The cloud top data [6] retrieved from the cloud-aerosol lidar on board were used as the ground truth in the verification despite studies had concluded that CTHs cannot be determined by satellite-borne lidar only and better results come from the combined use of radar and lidar [7]. For comparison, CTH data obtained using the HCAI algorithm by JMA [8] were also verified.

To evaluate the cloud top height estimations in deep convection which could pose threat to aviation safety, cases with $| T_{b,IR1} - T_{b,IR3} | < 3°C$ were studied. A common data set of all the available observations and CTH algorithms outputs at 00 min of every hour from July 2018 to Feb 2019 in the domain 20°S to 55°N, 80°E to 150°E were collected, accumulating a total number of around 1,750 data points.

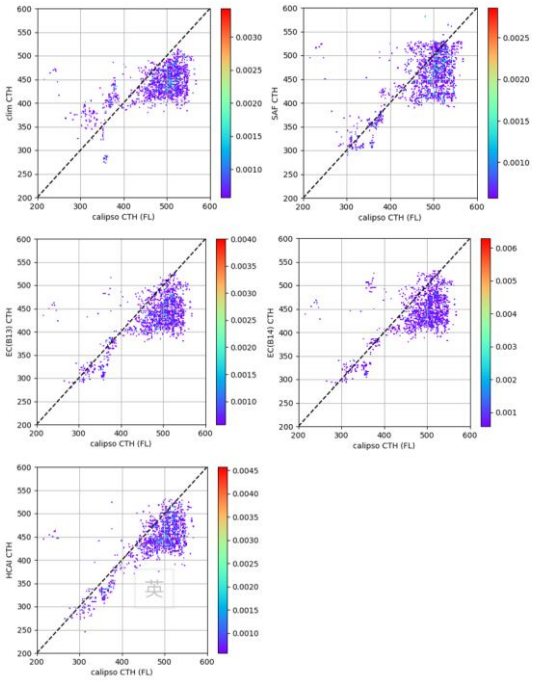

Figure 3: Relative frequency histogram of CALIPSO CTH observations (x-axis) and CTH derived from various methods (y-axis): (top left) climatological, (top right) SAF, (middle left) ECWMF B13, (middle right) ECMWF B14 and (lower left) HCAI.

Figure 3 shows the relative frequency histograms of CALIPSO CTH observations against the retrieved CTH by various algorithms. These plots show the general underestimation of the retrieved CTH in all algorithms over FL450. Below that level the retrieved CTH by the ECMWF models, SAF and HCAI performed reliably, except the climatological method (section 2.1) which slightly overestimates the CTH.

Table 1 shows a summary of the error statistics of the various algorithms. The results show that all algorithms underestimated the CTH with a negative mean error from -30 to -50 FL. Both ECMWF (B14) and ECMWF (B13) outperform the climatological method. SAF has the smallest Mean Error (ME) while SAF and HCAI were comparable to one another in terms of Mean Absolute Error (MAE) and Root Mean Square Error (RMSE).

Method	***ME***	***MAE***	***RMSE***
Climatological	-45	58	66
ECMWF (B13)	-51	57	67
ECMWF (B14)	-44	53	64
NWC SAF	-30	43	56
HCAI	-42	46	55

Table 1 Error statistics (in hundreds of feet) of the various CTH retrieval algorithms. (Mean Error: ME, Mean Absolute Error: MAE, and Root Mean Square Error: RMSE)

(b) Case studies

To further demonstrate the various performance of the ECMWF (B14), SAF and HCAI method, a case on 20th July 2018 at 04Z was illustrated in Figure 4. It shows the back scattered reflectivity (grey colour bars) of the laser beam by the clouds beneath CALIPSO's path (Figure 5). The top of the grey colour bar were treated as the cloud top height. From this figure, it can be seen that within the deep convection areas (7.5°N to 12°N), the three algorithms performed similarly with ECMWF (B14) and SAF slightly closer to the CALIPSO cloud top value than the HCAI value. Figure 5 shows that between 1°N to 5°N, there were only thin clouds depicted by CALIPSO. The true colour image on Fig.6 confirms that only thin patchy clouds existed over the area. SAF and ECMWF show more realistic result while HCAI significantly overestimated CTH in those areas. This case study reveals that other factors, such as the thickness of the clouds and etc., should also be taken into account before choosing an automatic algorithm for cloud top height retrieval.

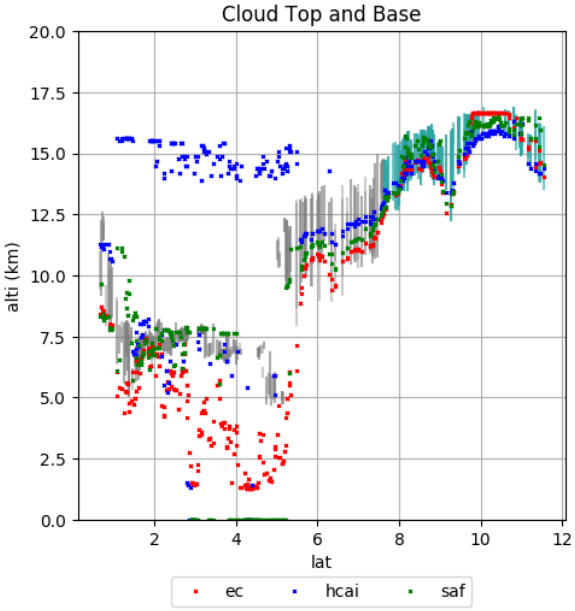

Figure 4 Vertical cloud profile of CALIPSO in grey colour. Greenish bar are the data points over deep convection determined by $| T_{b,IR1} - T_{b,IR3} | < 3°C$. CTH obtained by ECMWF algorithm (red), NWC SAF (green) and HCAI (blue) are plotted.

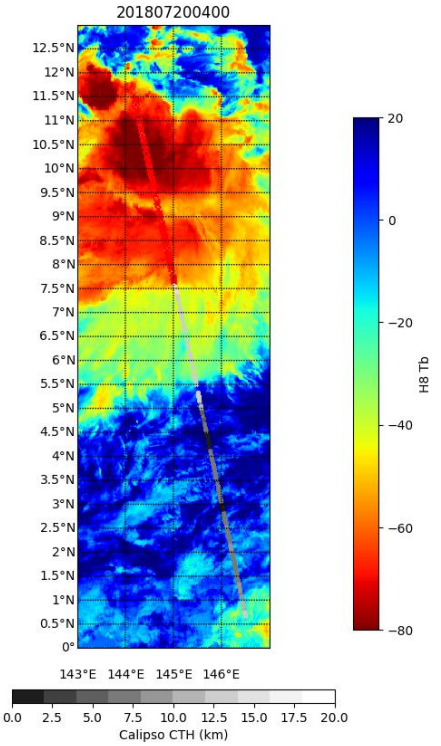

Figure 5 The corresponding CALIPSO track where the cloud profile in Fig.4 was extracted. Overlaid is the T_b (°C) of Himawari-8 B14 (11.2 μm) imagery. Red pixels on the tracks indicate deep convective clouds.

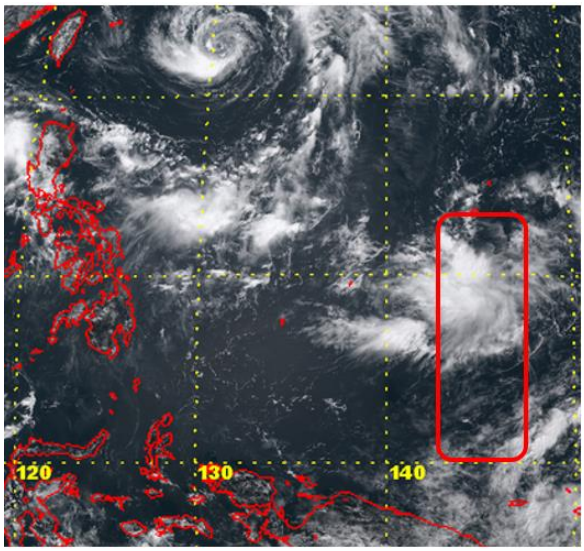

Figure 6 True colour image of Himawari-8. Red box indicates the area of the plot in Figure 5.

2.3 Applications and future work

We have studied several methods for estimating cloud top height and their performance against CALIPSO observations over an eight-months period. Verification results suggests that the ECMWF (B14) algorithm can improve CTH estimation against the climatological method. This could be attributed to the NWP model which takes into account the physical processes and variability of the atmosphere in the simulation. For deep convection case, SAF and HCAI perform comparably. In terms of computational efficiency, the ECMWF (B14) method was found to be the most efficient one and hence has been implemented in the HKO SIGMET Coordination web platform for routine operation (Figure 7).

Future work in the pipeline would include: collecting more data for further tuning and verification, optimizing the SAF algorithm for meeting the operational requirements, for the possibility of replacing the ECMWF (B14) method, and exploratory study of the redefinition of the CALIPSO cloud top height for deep convection suitable for aviation applications.

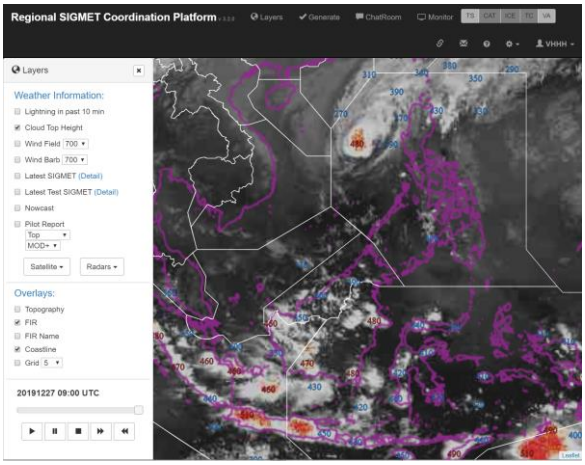

Figure 7 A screenshot of the HKO SIGMET Coordination platform with cloud top height (in FL) displayed in numbers on top of Himawari-8 deep convection satellite imagery.

3 SATELLITE NOWCASTING

Nowcasting of convection using satellite imageries is made possible in recent years by the availability of high resolution, rapidly updated multispectral imageries such as the Advanced Himawari Imager (AHI) on Himawari-8 satellite. Nowcasting for aviation applications requires a large geographical coverage where traditional ground-based radar nowcasting could not meet the requirements. Meanwhile, with the availability of global lightning dataset [9], significant convection areas could be depicted by incorporating the real time lightning data near/within a convective cloud.

Satellite nowcasting in our development of the SIGMET coordination platform was performed via the following steps:

(1) automatic identification of a convective system on multispectral satellite imageries in combination with global lightning activities (Sec.3.1);

(2) automatic tracking of the motions of the convective system by AI algorithms (optical flow in our case); and

(3) Nowcasting of the convective system in the next few hours ahead by semi-Lagrangian extrapolation scheme along the motion vector derived in step (2) above. [10]

Accurate detection and identification of the severity of significant convective clouds are one of the crucial steps in satellite nowcast. The following section discusses an enhanced method for the identification of significant convective system ((1) above) using the Himawari-8 multispectral imageries.

3.1 Satellite derived radar reflectivity algorithm

Previous study [11] has explored the technology for converting Himawari-8 multispectral imageries into

radar reflectivity using artificial neural network (ANN). In the previous study, the ANN was trained by correlating the four channels of the satellite (B08, B10, B13, B15) with the HKO radar CAPPI reflectivity. Any further satellite image could then be converted into "satellite-derived reflectivity" by inputting the 4 channel values into the ANN.

With the availability of broader coverage national radar mosaic from China, the above ANN was further enhanced by including broader coverage radar data in the training and testing process. Apart from that, information including the satellite location (w.r.t. the grid point of concern), local solar zenith, and a parameter describing seasonal variability were added into the ANN. As Visible and near-infrared albedos (B03, B04, B05) suffered from atmospheric attenuation, they were calibrated using the standard atmosphere [12] before adding into the neural network. These enhancements aimed to regularize the bias of remote sensing measurement due to off-sets from the sun and from the location of the satellite w.r.t. a pixel on the image. The enhanced algorithm has two neural networks, one using the non-visible channels which is applicable all day while the other including the visible channels which is only available during day time. To stitch the two modes together, a blending method making use of a weighting function depending on the diurnal parameter was utilized to avoid apparent strengthening/weakening of the blended algorithm when switching from one mode to another in the course of time. The enhanced algorithm thus uses 7 satellite channels instead of 4 with the addition of 3 visible channels.

3.2 Performance

The performance of the enhanced algorithm was compared with the original algorithm. The satellite derived radar reflectivity were checked against the national radar mosaic. The training and the verification dataset covered August, September and December in 2018 at the common measurement time of radar and satellite. Odd hours data were used for the training while even hours data were used for verification. Grid-based verification with grid size of around 4km was performed for various radar reflectivity thresholds. Table 2 shows the contingency table where the Critical Success Index (CSI) was used,

$$\mathrm{CSI} = \frac{H}{H+M+FA} \qquad (2)$$

	Derived reflectivity ≥ threshold	Derived reflectivity < threshold
Measured reflectivity ≥ threshold	Hit H	Miss M
Measured reflectivity < threshold	False Alarm FA	Correct Negative CN

Table 2 Contingency table for grid-based verification

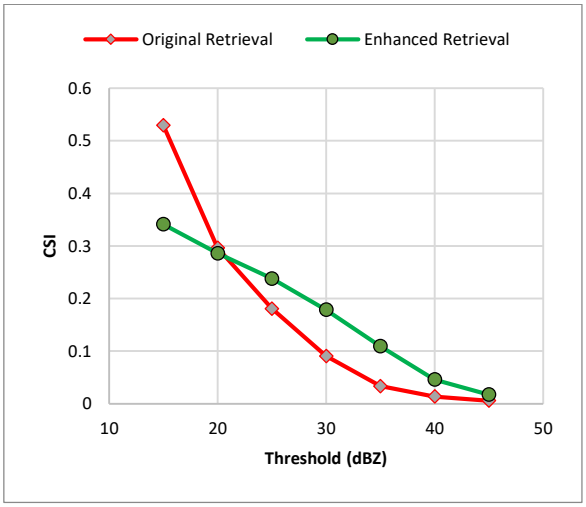

Figure 8 The CSI performance of the enhanced satellite derived radar reflectivity ANN compared with the original ANN.

Figure 8 shows that the CSI of the enhanced ANN consistently outperformed the original one for reflectivity of over 20 dBZ. This suggests that the enhanced ANN could better capture and detect significant convection at higher reflectivity values. This could be attributed to the broader coverage of radar in the training, addition of new parameters in the network and the inclusion of visible channels in the ANN.

Figure 9 shows a case of the derived radar reflectivity retrieved for TC Mangkhut over Northwest Pacific and south China Coast in September 2018. The intensity and coverage of the spiral rain bands were well be captured by the enhanced ANN. Nonetheless, some small features which were observed on radar were not resolved and some intense areas near the coast were retrieved properly. This could be due to the difference in the resolution of the satellite and radar data. Meanwhile, the thick high clouds in a typhoon may also have masked some of the features that could only be observed via ground-based radar.

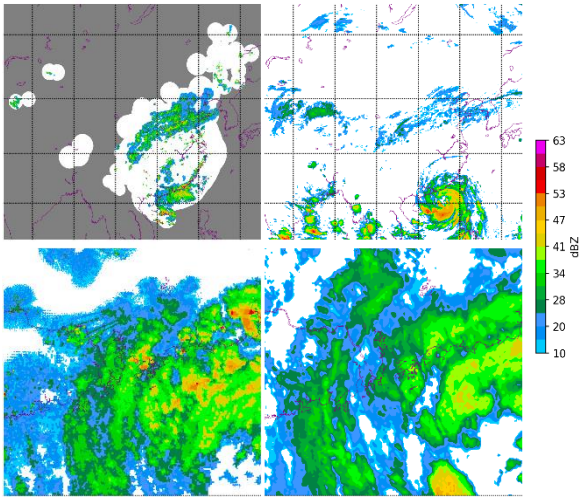

Figure 9 TC Mangkhut on 15 Sep 2018 striking the south China Coast. Left Column: China national radar mosaic composite reflectivity; Right Column: Satellite-derived reflectivity; Upper Row: Mainland China; Lower Row: Vicinity of Hong Kong

3.3 Future work and limitations

The above study suggests that the enhanced satellite derived reflectivity ANN outperformed the original one. Further work on performing nowcast and related verification are on-going. Although the radar coverage has been expanded, case studies still suggest that the derived reflectivity over the tropical areas could sometimes be overestimated. Further enhancements such as the inclusion of more radar data over those areas in the ANN training phase would be pursued. Further verification metrics would continue to be explored.

4 SUMMARY AND CONCLUSIONS

This paper discusses the applications of high resolution, rapidly updated multispectral satellite images, NWP data and AI technology for the detection and analysis of significant convective clouds for aviation applications. Several cloud top height algorithms were compared. Application of AI on retrieving radar reflectivity from multi-spectral satellite were also enhanced and evaluated. These studies laid the foundations for the operation of the HKO SIGMET Coordination platform for hazardous weather monitoring and warnings services in the Asia Pacific region.

ACKNOWLEDGEMENTS

The authors would like to thank Ms S.Y. Lau and Dr P.W. Li for their valuable comments on the research project and the abstract.

REFERENCES

[1] International Civil Aviation Organization. (1993). *Manual of the ICAO Standard Atmosphere (extended to 80 kilometres (262 500 feet))* (Third ed.).

[2] Donovan, M.F., E.R. Williams, C. Kessinger, G. Blackburn, P.H. Herzegh, R.L. Bankert, S. Miller and F.R. Mosher (2008). The Identification and verification of hazardous convective cells over Oceans using visible and infrared satellite observations. *J. Appl. Meteor. and Climatol.* **46**, 164-184.

[3] Bessho, K., and Coauthors, (2016): An introduction to Himawari-8/9—Japan's new-generation geostationary meteorological satellites. *J. Meteor. Soc. Japan*, **94**, 151–183

[4] Herve Le GLeau, (2019): *Algorithm Theoretical Basis Document for the Cloud Product Processors of the NWC/GEO*. <http://nwcsaf.org/Downloads/GEO/2018/Documents/Scientific_Docs/NWC-CDOP2-GEO-MFL-SCI-ATBD-Cloud_v2.1.pdf>

[5] Saunders, R., Hocking, J., Turner, E., Rayer, P., Rundle, D., Brunel, P., Vidot, J., Roquet, P., Matricardi, M., Geer, A., Bormann, N., and Lupu, C., (2018): An update on the RTTOV fast radiative transfer model (currently at version 12), Geosci. Model Dev., **11**, 2717-2737.

[6] Vaughan, M., Young, S., Winker, D., Powell, K., Omar, A., Liu, Z., Hu, Y., and Hostetler, C. (2004). Fully automated analysis of space-based lidar data: an overview of the CALIPSO retrieval algorithms and data products. *Proc. SPIE*, **5575**, pp. 16-30.

[7] Hagihara, Y., H. Okamoto, and Z. J. Luo (2014), Joint analysis of cloud top heights from CloudSat and CALIPSO: New insights into cloud top microphysics, J. Geophys. Res. Atmos., 119, 4087–4106.

[8] Mouri, K., H. Suzue, R. Yoshida, and T. Izumi, (2016): Algorithm Theoretical Basis Document of Cloud top height product. Meteorological Satellite Center *Technical Note*, **61**, 33-42

[9] Vaisala Global Lightning Dataset GLD360, (2014). < https://www.vaisala.com/sites/default/files/documents/WEA-MET-GLD360%20Datasheet-B210800EN.pdf>

[10] Woo, W. C., & Wong, W. K. (2017). Operational application of optical flow techniques to radar-based rainfall nowcasting. *Atmosphere*, **8(3)**, 48.

[11] Woo, W. C., Ip, Y. Y., Wong, W.K. & Chan, N.H. (2017). Development of Satellite Reflectivity Retrieval Technique for Tropical Cyclone Rainfall Nowcasting. *Fourth International Workshop on Tropical Cyclones Landfall Processes* (IWTCLP-4), Macau, China, 5-7 December 2017

[12] Kasten, F., & Young, A. T. (1989). Revised optical air mass tables and approximation formula. Applied optics, **28(22)**, 4735-4738.